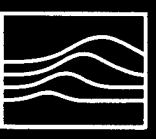

Mission Research Corporation

MRC/WDC-R-393

DESIGN AND DEVELOPMENT OF A PLASMA WAKEFIELD KLYSTRON

Final Report

December 23, 1996

Authors: John Pasour
David Smithe
Robert Seeley
Khanh Nguyen

Prepared for: U.S. Army Research Laboratory
2800 Powder Mill Road
Adelphi, MD 20783-1197

Contract No. DAAL01-93-C-0053 (MRC-93086)

Prepared by: MISSION RESEARCH CORPORATION
8560 Cinderbed Road, Suite 700
Newington, VA 22122

MRC/WDC-R-393
Copy No. 2

DESIGN AND DEVELOPMENT OF A PLASMA WAKEFIELD KLYSTRON

Final Report

December 23, 1996

Authors: John Pasour
David Smithe
Robert Seeley
Khanh Nguyen

Prepared for: U.S. Army Research Laboratory
2800 Powder Mill Road
Adelphi, MD 20783-1197

Contract No. DAAL01-93-C-0053 (MRC-93086)

Prepared by: MISSION RESEARCH CORPORATION
8560 Cinderbed Road, Suite 700
Newington, VA 22122

TABLE OF CONTENTS

LIST OF FIGURES

EXECUTIVE SUMMARY

During this SBIR program, we have investigated a novel microwave source that utilizes a plasma to bunch the electron beam. The electron beam interacts with the plasma via the wakefield produced by the head of the electron beam as it passes through the plasma. The resulting plasma oscillations bunch the beam at a frequency proportional to the plasma frequency. Thus, the device can be tuned by varying the plasma density. The theory of the device has been developed, and numerical simulations of the interaction have been performed. The simulations have covered a very broad parameter range, including multi-GW electron beams at an energy of about 0.5 MeV as well as 100-keV electron beams at current levels of 100 to 500 A (10 to 50 MW). Practical problems, such as voltage droop during the pulse and non-uniform plasma density, have been addressed in the simulations to obtain an idea of the robustness of the device.

The bulk of the Phase II program has been devoted to a proof-of-principle experiment designed to validate the theory and simulations. The experimental device uses a 100-keV electron beam from a Febetron pulse generator coupled to a velvet cathode. An adjustable-length plasma chamber was fabricated inside a larger, existing vacuum chamber. Diagnostics to measure the plasma density profile, beam voltage, and beam current at various locations were implemented. In particular, fast, low-inductance Faraday cups and small B-dot loops were used to measure beam modulation and cavity excitation directly, thereby allowing a comparison of bunching amplitude and frequency with plasma density and interaction length. These experiments have demonstrated convincingly that strong electron bunching can be produced over a distance of about 10 to 15 cm in a plasma of density $\sim 10^{10}$ cm^{-3}. The beam bunching frequency can be varied by about a factor of two simply by varying the plasma density, in excellent quantitative agreement with theory. To demonstrate the extraction of RF energy from the bunched beam, a single klystron-like cavity was placed downstream of the plasma interaction region. With this simple cavity, the bandwidth was limited by the cavity Q. As predicted, strong beam coupling to the cavity was observed when the bunching frequency was within the cavity bandwidth.

In this report, we will discuss the theory, simulations, and experiment. The body of the report is in the format of a journal manuscript, which we have submitted to the Journal of Applied Physics. Additional experimental results are included in an appendix.

1. INTRODUCTION

The plasma wakefield klystron (PWK) is a unique plasma-based oscillator. It is comprised of a plasma-filled chamber, which provides beam bunching, and an RF extraction circuit, which in this initial version consists of one or more resonant cavities, as in a conventional klystron. Other embodiments of the device could substitute an appropriate slow-wave circuit (e.g., a helix, as in a traveling wave tube) for the cavity structure. The bunching mechanism in the PWK is the plasma wakefield phenomenon, which has been experimentally observed and studied in conjunction with intense relativistic beam transport in plasma channels [1]. Key features of the interaction are the ability to tune the bunching frequency by simply varying the density of the plasma and the ability to propagate and bunch very high electron currents, because of the space-charge neutralization provided by the plasma.

In the earlier beam propagation experiments, the plasma wakefield bunching mechanism was observed when a high-power electron beam was propagated through a narrow plasma channel in the presence of a diffuse background plasma. Without the diffuse background plasma, the beam head simply expelled the plasma channel electrons, leaving behind massive ions to focus and guide the beam body. This is known as the ion-focused regime (IFR) electron-beam transport. It has been successfully used as an efficient transport mode in a wide variety of experiments at Lawrence Livermore National Laboratory (LLNL) [2], Sandia National Laboratories (SNL) [3], and Naval Surface Warfare Center (NSWC) [4]. The plasma channel formation in these experiments is accomplished either by injecting an excimer (KrF) laser beam or a low-energy (~200 eV) electron beam into a low-pressure neutral gas prior to the injection of the high-power electron beam.

This relatively simple picture of IFR transport changes somewhat in the presence of the diffuse background plasma used in the PWK. In this case, there are excess electrons in the background plasma that are not expelled by the beam head, but they are perturbed. These excess electrons lie outside the charge neutralization radius, which is the point at which the total enclosed line density of the channel and background ions is equal to the electron beam line density. The perturbed electrons begin to oscillate at the characteristic frequency of the background plasma, and these oscillations create an electrostatic standing wave pattern (wakefield) in a reference frame moving with the beam. This standing wave accelerates and decelerates beam electrons, which leads to modulation of the beam energy and current at the background oscillation frequency. Thus, the PWK operating frequency is essentially the plasma frequency corresponding to the background plasma density, n; i.e., $\omega \approx \omega_p = (4\pi ne/m)^{1/2}$,

where $-e$ and m are the electron charge and mass, respectively. As we will discuss below, there is a small geometric correction to this infinite-plasma expression.

The potential of the plasma wakefield effect to strongly modulate (bunch) the electron-beam current was first suggested by an experiment performed at NSWC [1]. In this experiment, a 1.6-MeV, 1-kA electron beam having a 5-nsec rise time and 15-nsec flat top was injected onto a plasma channel, preformed with a KrF excimer laser, inside a drift tube 25 cm in radius and 3.6 meters in length. The drift tube contained a uniform diffuse plasma of density 2×10^9 cm^{-3} created by a hot filament discharge in low-pressure trimethylamine (TMA) gas. Strong current modulation was observed at the end of the 3.6-meter chamber, clearly demonstrating the potential of the plasma wakefield to bunch the beam. The experimental results were in excellent agreement with numerical simulations performed by MRC in support of the experiments. Moreover, both experimental and numerical results confirmed the linear scaling of the beam bunching frequency with respect to the diffuse plasma frequency.

The NSWC experiments were performed to study exo-atmospheric electron beam propagation and were motivated by a concern of possible damaging effects the ionospheric plasma and other plasma sources may have on long-range electron-beam propagation. Thus, the goal was to minimize the beam modulation or disruption by the plasma interaction. For the PWK high-power microwave generation concept, the goal is to maximize the plasma wakefield effect to provide an extremely strong and efficient mechanism for electron-beam bunching. A related beam buncher for accelerator applications was recently analyzed by Katsouleas et al. [5]. In this case, a laser-driven plasma wakefield oscillation is used to prebunch an electron beam prior to acceleration.

2. WAKEFIELD MECHANISM

When a beam first passes through a plasma, it expels plasma electrons from its path because of its space charge. When the plasma density exceeds that required to screen the beam's potential, a plasma oscillation is excited in the plasma electrons by the initial beam-pulse transient (beam head). These radial oscillations of the excess plasma electrons induce an electrostatic wakefield wave with a phase velocity equal to the beam front velocity. The plasma wave is excited along the entire length of the beam path wherever the plasma density is sufficiently high. In general, plasma oscillations are very weakly-damped, predominantly stationary waves at the densities, temperatures, and time scales of interest here. Therefore, each small section of plasma oscillates in a predominantly radial direction at fixed axial position, with little communication between neighboring sections of plasma along the beam path. Conse-

quently, in the beam frame each beam segment is under the constant acceleration or deceleration of a static axial electric field. This is the process that leads to beam-energy modulation and eventually beam-current modulation (bunching).

The above discussion suggests that the amplitude of energy modulation initially rises uniformly with the time the beam spends in the plasma. This implies that the length of the wakefield chamber is the most important parameter governing the amplitude of beam bunching. To illustrate the interaction in the high-power (>1 GW) regime, we present results of a numerical simulation using the particle-in-cell code, MAGIC [6], in which an electron beam (500 keV, 5 kA, 15-nsec rise time) is injected into a simple cylindrical cavity, of radius 25 cm and length 22.5 cm, filled with background plasma. The background plasma density is 2×10^{10} cm^{-3}, with a smaller coaxial channel of 2.5-cm radius containing twice that density. This small channel corresponds to an IFR channel that could be used to transport the intense electron beam over the entire interaction region. Plasma oscillations are established quickly as the beam is injected. Observations of the beam current and energy made at four locations along the beam path (z = 1, 7, 13, and 19 cm) clearly show the growing current and energy modulation, as illustrated in Fig. 1. The plasma wakefield oscillations establish an energy modulation; hence, the bunching is initially more evident in the beam power signal than in the current alone.

Figure 2 shows a graph of the observed bunching amplitude in current and energy as a function of distance in the wakefield chamber for the simulation of Fig. 1 at time t = 25 nsec. This is after the dissipation of a transient effect, particularly evident in the current bunching, that occurs near the end of the 15-nsec rise of the injected current pulse. Both the current and energy bunching amplitudes increase nearly linearly with axial distance up to z = 19 cm. However, when the length of the wakefield chamber is further increased, the energy of certain properly phased beam electrons can be modulated all the way down to zero, thus essentially stopping a portion of the beam altogether. An example of such an over-modulated beam is shown in the phase space plot of Fig. 3. In this simulation, the plasma chamber length has been increased to 60 cm. The point of beam stoppage occurs at about 30 cm into the chamber. Reflected electrons are clearly evident in the phase-space plot.

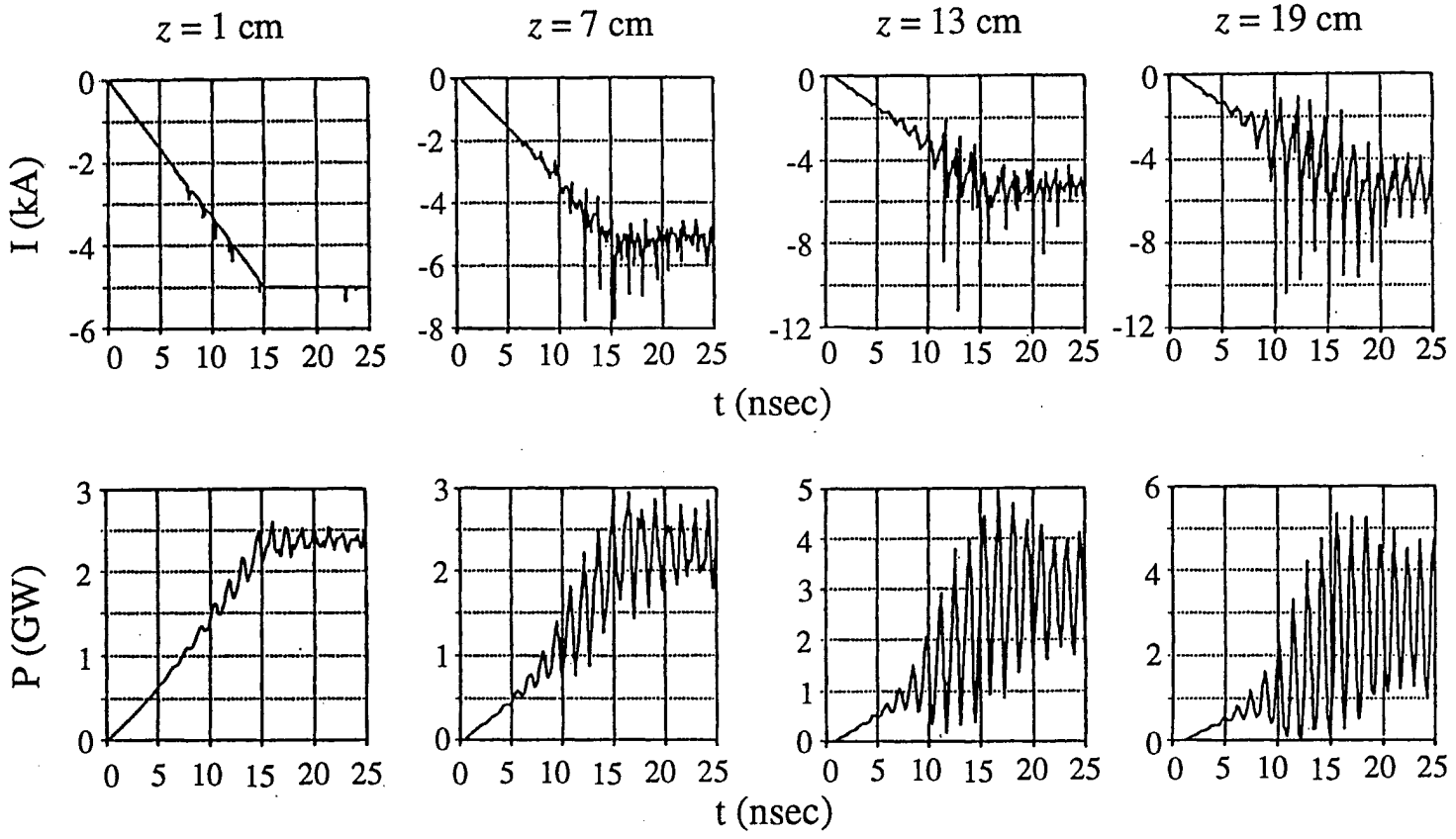

Figure 1. Beam current and power modulation at $z = 1$, 7, 13, and 19 cm inside wakefield chamber.

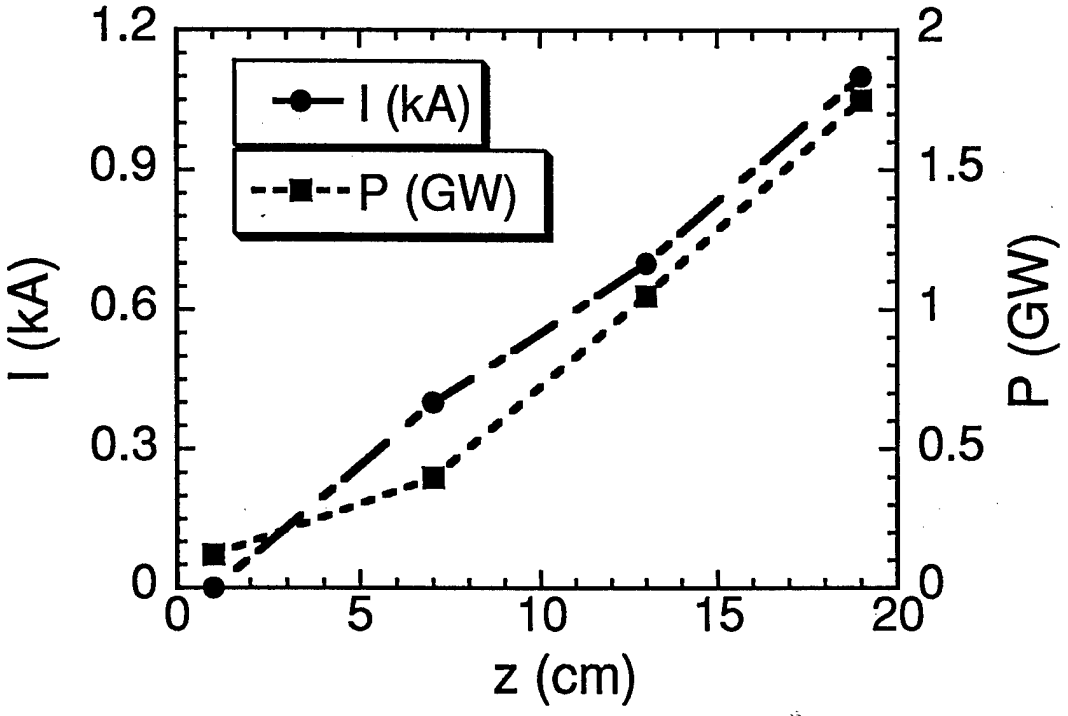

Figure 2. Amplitude of beam current and power modulation vs. axial position at t = 25 nsec.

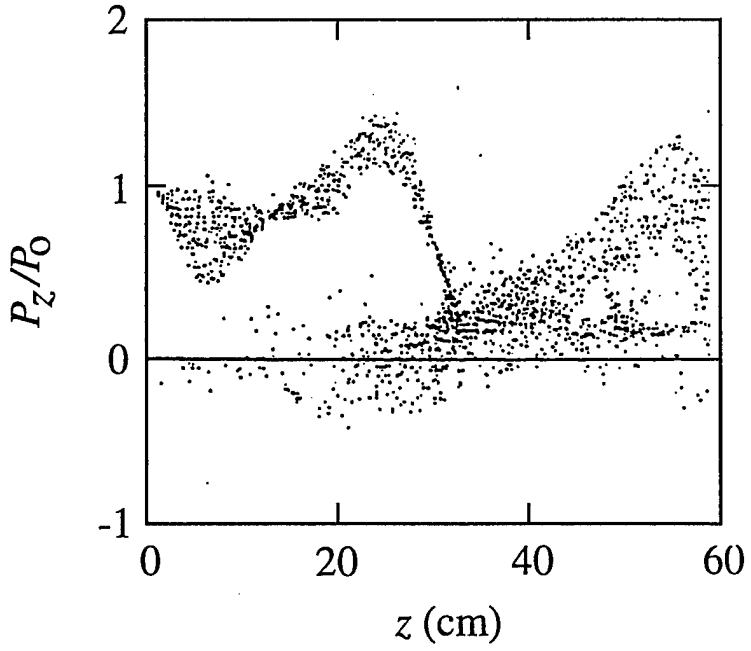

Figure 3. Phase space diagram showing beam electrons' axial momenta and positions at t = 25 nsec in a 60-cm-long plasma chamber.

Fourier transforms of the power and current measured at z = 19 cm in the simulation of Fig. 1 show a dominant frequency at 750 MHz, as shown in Fig. 4. Close inspection of the current waveform in Fig. 1 shows that the current bunches have a sawtooth shape with a steeper rise portion, which indicates the presence of a significant first harmonic component, plainly evident in the Fourier transform. This harmonic component is typical of energy-bunched beams, in which both the velocity and density tend to have pure oscillation forms. The current density product, $J = qnv$, therefore contains a first harmonic. Energy in harmonics cannot be converted directly to microwave power at the fundamental, so it is more revealing to examine the beam energy or power modulation, which shows negligible harmonic content.

To demonstrate incontrovertibly that the wakefield effect is the origin of the beam bunching observed above, the results of a simulation performed without the background plasma, but with the small-diameter plasma channel, are shown in Fig. 5. Without the background plasma, there should be no wakefield, and hence one would expect no bunching. Indeed, the current and energy traces for this simulation, measured at the same final location as the previous case, show no indication of bunching nor a preferred frequency, although there is a significant amount of noise on the beam. This simulation demonstrates that the presence of the plasma is necessary for the bunching to occur, as asserted above.

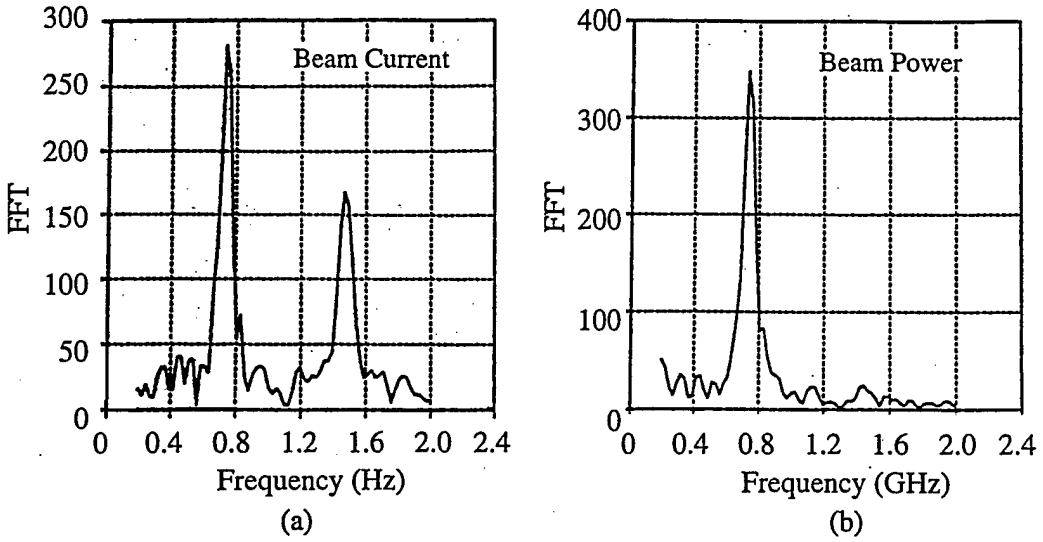

Figure 4. FFT spectra of beam current (a) and power (b) at z = 19 cm.

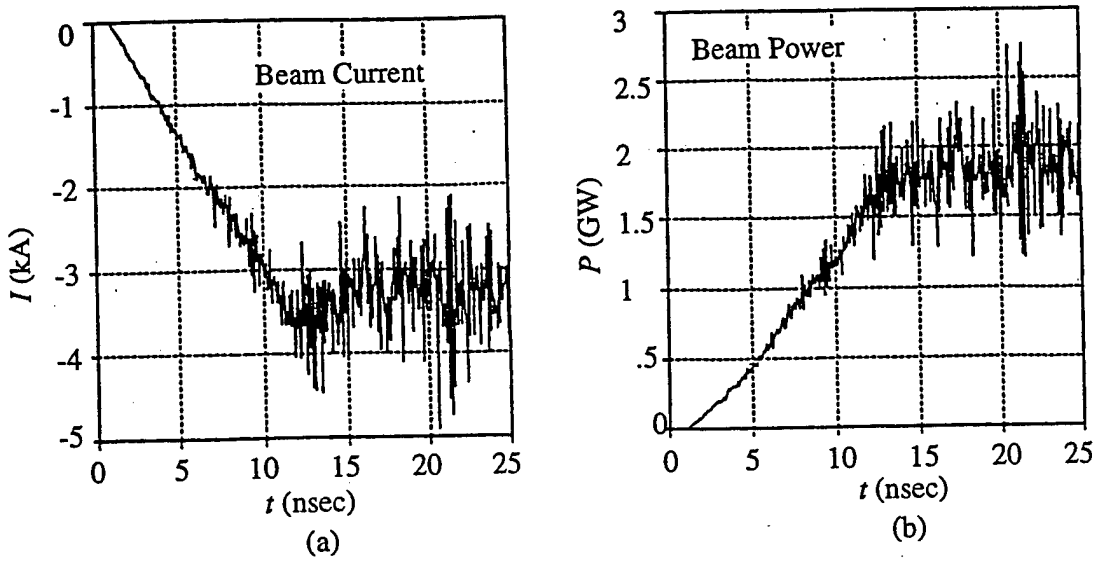

Figure 5. Beam current (a) and power (b) at z = 19 cm with IFR channel but no background plasma.

As discussed in Ref. 1, and as should be clear from the above description of the plasma wakefield oscillations, the frequency of the modulation should be near the plasma frequency of the background plasma. For radial oscillations in a cylindrical plasma, the oscillations occur at a frequency of $\omega_p/\sqrt{2}$ [7]. For all of the cases shown in the previous figures, the plasma density is 2×10^{10} cm^{-3}, which corresponds to an oscillation frequency of 900 MHz. The observed frequency is in the range of 750 to 850 MHz, which is 5-15% lower than predicted. However, it is likely that the actual plasma frequency may be reduced by the finite size of the wakefield chamber, particularly for the parameter range of interest here, where the wavelength of the wakefield oscillations is on the same order as the size of the chamber [8].

3. OPTIMIZATION FOR MICROWAVE PRODUCTION

The two fundamental parameters of the wakefield bunching mechanism, namely the plasma density and the length of the chamber, can be adjusted over a rather wide range to obtain the desired frequency and optimal bunching for microwave production. The length of the chamber should be selected so as to provide a large bunching amplitude, but not quite so large as to cause the amplitude to saturate at the full beam energy. Thus, the chamber length is determined by the axial electric field in the plasma that produces the beam modulation. Figure 6 shows the axial electric field for the simulation of Fig. 1, both over the full length of the wakefield chamber at fixed time (14 nsec) and radius (4 cm) and also at a fixed location (z = 15 cm, r = 2.5 cm) for the entire

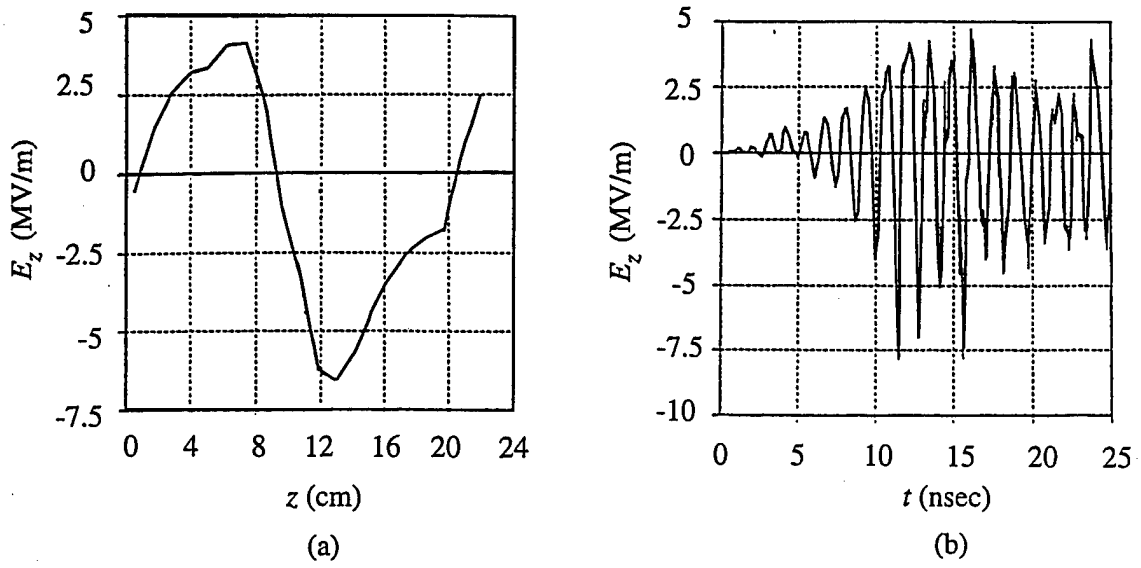

Figure 6. Axial electric field. (a) Field vs. axial position at t = 14 nsec. (b) Field vs. time at z = 15 cm.

time history of the simulation. This simulation shows the peak electric field to be about 3 to 4 MV/m at the beam radius.

An additional physical process that may affect the rate at which the bunching amplitude increases, as well as the phase stability of the bunching process, is the excitation of propagating space-charge waves in the beam itself. Friedman et al. [9] concluded that this effect should aid the bunching process in their work on intense-beam relativistic klystrons. It is also possible that the plasma interaction with the space-charge waves in the beam may allow some small degree of communication between axial positions, thereby aiding the phase stability of the entire bunching process.

Extraction of RF energy from the electron beam can proceed much as in conventional microwave sources. However, the beam must first be removed from the plasma to prevent shorting of the RF fields in the extraction region. Beam transport in the vacuum region can be achieved either by providing a narrow plasma channel (IFR transport) or by a suitable magnetic focusing channel. The former approach is naturally compatible with the plasma bunching mechanism, but there are serious questions regarding the leakage of channel electrons to the RF structure and subsequent breakdown. Because the channel electrons are ejected prior to the build-up of RF field in the cavities, careful design and surface preparation should allow one to avoid breakdown, but this remains to be proven at high power levels. Magnetic focusing has

the advantage of eliminating the plasma from the extraction region but introduces problems of matching the beam from the plasma into the magnetic focusing channel and of confining the plasma to the bunching chamber.

Regardless of the vacuum transport mechanism, the transition from plasma to vacuum for intense electron beams is complicated by the space-charge fields of the beam. To illustrate the process for the situation described above, a simulation is presented in which a 7-cm-radius drift tube has been added to the end of a 20-cm-long, 25-cm-radius wakefield bunching chamber. An IFR transport channel is used throughout the entire interaction length, with the same beam, plasma, and channel parameters as in Fig. 1. In the simulation, there is a sharp boundary of the background plasma at the edge of the plasma chamber. Beam current and power for this configuration are shown just before and just after the transition from plasma chamber to drift tube in Fig. 7. At the end of the plasma chamber, the beam power modulation amplitude is near 65%, while the current bunching is about 30%. Just inside the drift region, the power modulation is substantially reduced as the beam contributes to the field energy in the empty portion of the drift tube. Additional field energy is required in the vacuum region because of the lack of screening provided by the plasma. The transition occurs such that the high energy portion of the beam loses energy to the static fields while the low-energy portion of the beam gains energy. The result is that the power modulation amplitude drops rapidly from 65% to 30%. The current bunching is essentially unaffected by the transition, however, and preserves its 30% amplitude.

Following the transition to the drift region, the beam exhibits ballistic bunching in the usual manner of a klystron. In addition, the beam space-charge waves affect the ballistic bunching rate significantly, even more than in the wakefield chamber. The bunching is observed to increase for about 10 to 15 cm, after which it saturates when the fast electrons in the bunch overtake the slow electrons. The bunching amplitudes for both power and current rise from about 30% to 50%. The physical location of the maximum bunching is relatively insensitive to the original beam-bunching amplitude, due probably to the beam space-charge wave effects.

Coupling the power from the beam has been simulated by employing multiple klystron-like interaction cavities. As much as 1.1 GW of RF power has been extracted from this beam using a 6-cavity configuration, as shown in Fig. 8. This corresponds to an efficiency of about 40%. By contrast, a single cavity, placed at the point of maximum bunching, can extract only about 20% of the energy from the beam. The simulation of Fig. 8 uses a 550-keV, 5-kA beam having a 15-nsec rise time, 85-nsec flat top, and 15-nsec fall time. The RF output from the 90-cm-long cavity structure (which consists of an

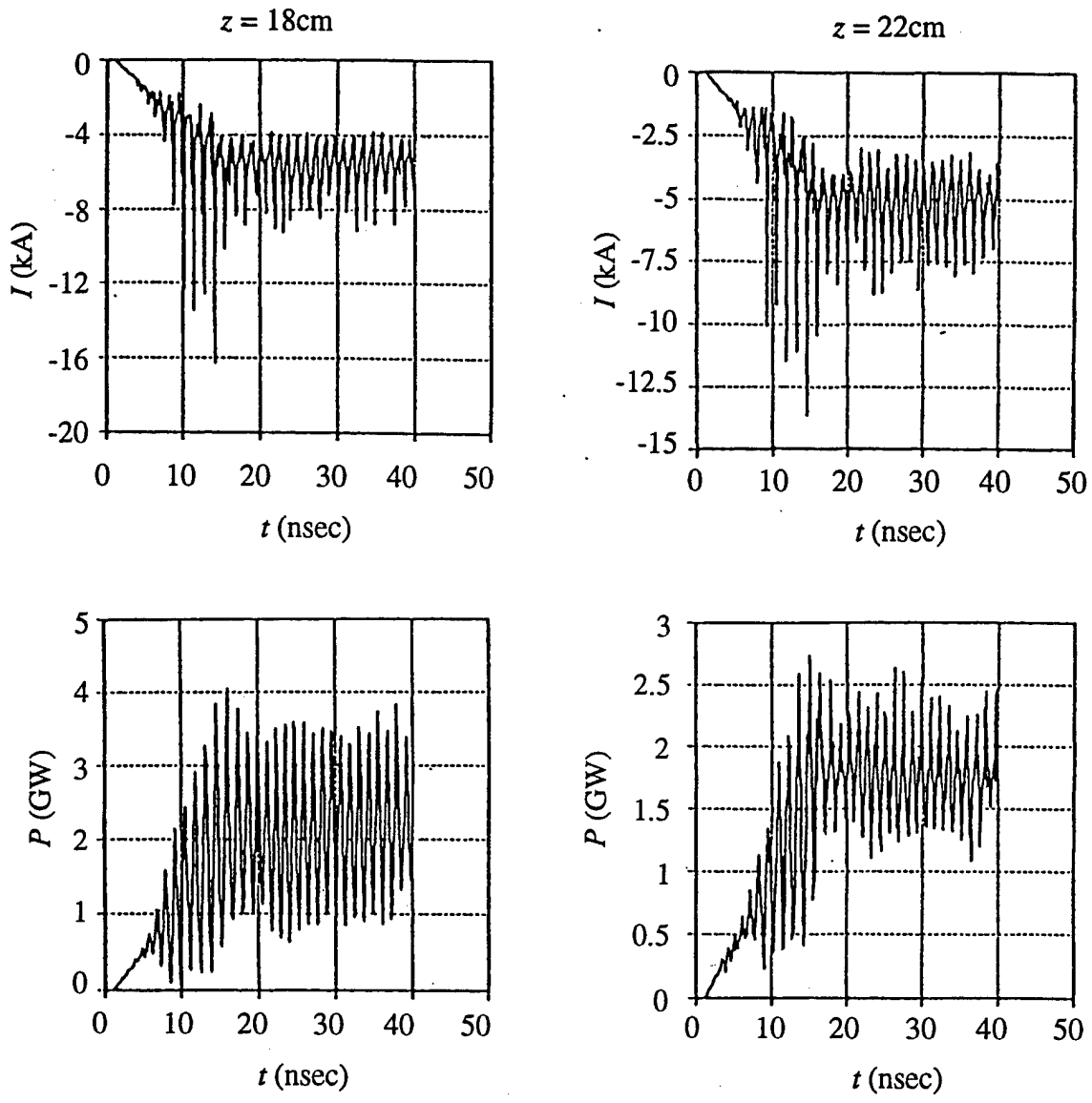

Figure 7. Beam current and power on each side of transition from plasma chamber to vacuum drift tube.

idler cavity followed by two extraction cavities followed by another idler cavity and two more extraction cavities) continues to increase for about 25 nsec after the beam current reaches its peak as the cavities fill with RF energy. The output then saturates at the 1.1-GW level. However, the power begins to decrease unexpectedly about 25 to 30 nsec before the end of the beam current and voltage flat top. This 20% decrease is apparently due to some electrons, either those ejected from the plasma channel or primary beam electrons, being reflected and accelerated back toward the plasma chamber, taking energy from the cavities along the way. Nevertheless, this simulation illustrates the potential of the PWK as a very high power microwave source.

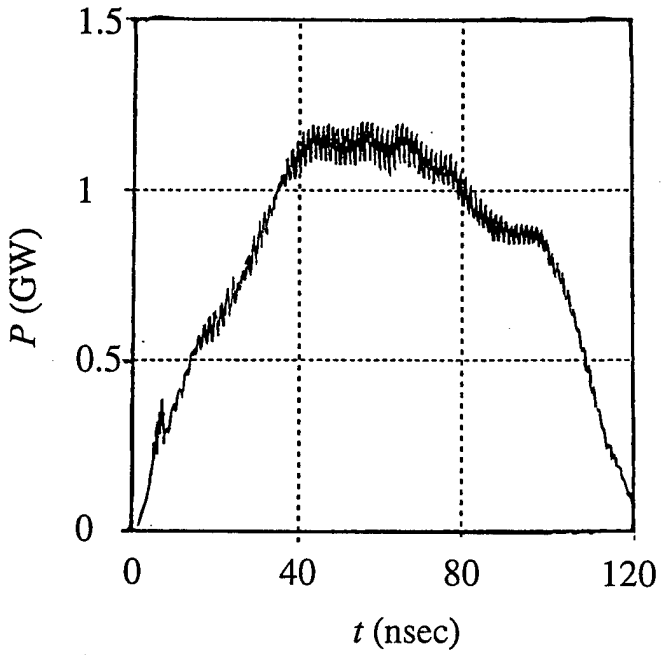

Figure 8. RF output power vs. time for a 6-cavity klystron output coupler.

Lower Power Operation

In addition to the high-power simulations discussed above, several lower power configurations have been studied to more closely correspond to the available electron beam generator used in the proof-of-principle experiments. Besides the lower beam energy (~100 keV) and current (0.2 - 1 kA), the major difference in these simulations is the addition of various non-ideal effects, such as a time-varying beam voltage and plasma density gradients. Also, simulations have been performed to study the replacement of the IFR plasma channel for beam transport by solenoidal lenses in the vacuum regions. Because simulations of the plasma wakefield bunching mechanism show that even a small (50-100 G) axial magnetic field in the plasma chamber significantly degrades beam bunching by restricting the radial plasma oscillations, care must be taken to shield the transport field from the plasma. This is accomplished by using shielded coils in an alternating configuration. In principle, periodic permanent magnet focusing could also be implemented.

First, we present a baseline simulation, using ideal beam injection and a uniform background plasma in addition to a gaussian plasma IFR channel. The 100-keV, 200-A, 5-cm-diameter beam is injected with purely axial energy into an 8-cm-diameter tube 30 cm from the plasma chamber, which has a 30-cm diameter and 11.2-cm length. The current at the downstream end of the plasma chamber is essentially fully modulated, as shown in Fig. 9. There is a significant first and second harmonic content in addition to the 1.05-GHz fundamental. To determine the importance of voltage flatness, this same simulation is repeated with a beam voltage that decreases linearly from the peak of 100 keV to 80 keV at 30 nsec into the pulse. The results are summarized in Fig. 10, which shows the amplitudes of the FFT at the fundamental frequency for the two cases at three axial positions relative to the center of the plasma chamber. This graph shows the decrease in modulation strength as the beam emerges from the plasma as well as the general degradation in bunching with the drooping voltage pulse. Here and in the following FFT plots, the FFT amplitude for each quantity is normalized by dividing by the unmodulated value (e.g., 200 A or 2×10^7 W) and multiplying by the fundamental frequency. The axial distance is measured from the center of the plasma chamber. Note that since the beam is almost completely modulated at the output of the plasma chamber, no additional ballistic bunching occurs in the vacuum drift region in this case.

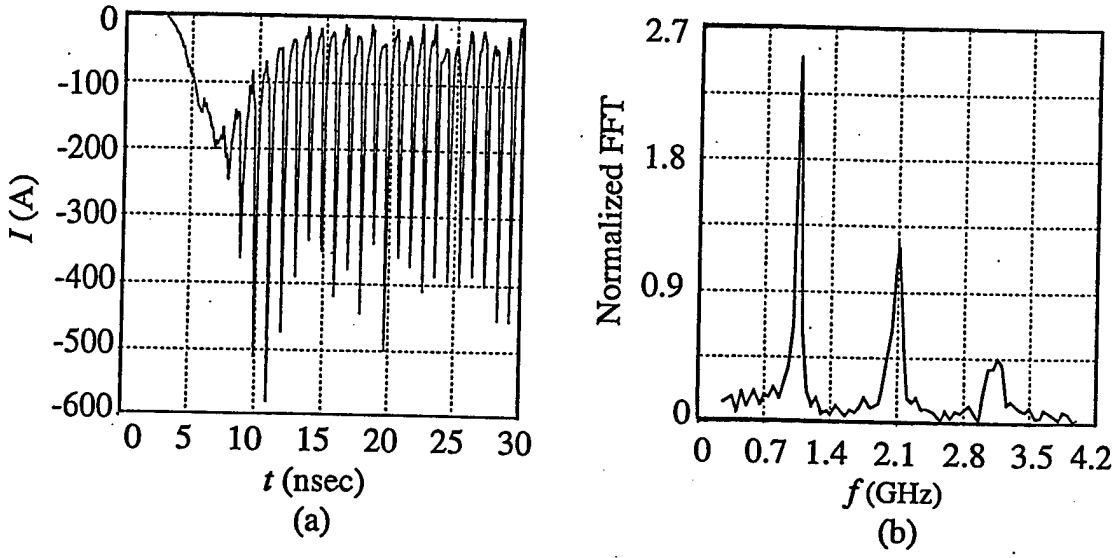

Figure 9. Modulation of a 100 keV, 200-A beam at z = 11 cm. (a) Current vs. time. (b) FFT of current.

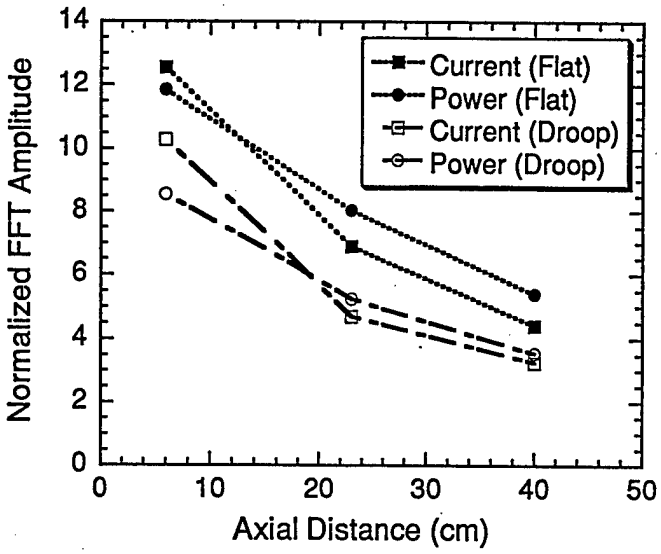

Figure 10. Variation of beam modulation with axial distance for a flat voltage pulse and one that droops by 20% over 30 nsec.

Results from additional simulations to study effects of plasma density gradients, plasma leakage out the ends of the chamber into the vacuum beam tube, and plasma chamber geometry are summarized in Fig. 11, which shows normalized FFT current amplitudes. In all these cases, the beam energy is still 100 kV, but the current has been increased to 500 A. The base configuration is essentially the same as that used in Fig. 9, but the plasma chamber length is 15 cm. The "flanged end" configuration uses a 20-cm-long plasma chamber that is terminated 5 cm from the downstream end by a thin flange that extends from the 4-cm-radius of the vacuum tube wall to a radius of 7.6 cm. The flange is supported on a cylinder that effectively extends the downstream vacuum tube wall. The purpose of this configuration is to provide a simple means of adjusting the chamber length experimentally by varying the length of the cylinder. The radial plasma gradient is of the form $n(r) = n_0 (1+r/r_w)$, where r_w is the outer radius of the plasma chamber. The axial gradient is of the form

$$n(z) = n_o\left[1-\left(\frac{z-z_0}{L/2}\right)^2\right],$$

where z_0 is the center of the chamber and L is the chamber length. The plasma leakage case is of the same form, but with $L/2$ replaced by L. Thus, the "axial gradient" profile goes to zero at the chamber end walls, while the "axial leakage"

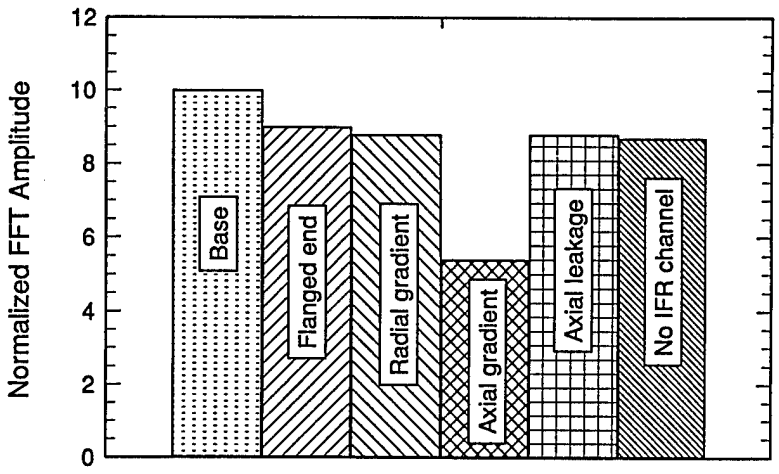

Figure 11. FFT amplitude of beam current for several different configurations.

profile extends $L/2$ into the vacuum beam tube. Generally, plasma gradients are found to have a deleterious effect, but the effect is relatively minor until a drastic gradient is imposed (i.e., plasma density decreasing completely to zero at the chamber wall). Also, eliminating the IFR plasma channel and injecting the beam 3 cm from the edge of the plasma chamber has relatively little impact on the bunching for the current level here. Of course, additional focusing would be required to transport the beam downstream of the plasma chamber.

4. EXPERIMENT

The proof-of-principle experiment is shown schematically in Fig. 12. It consists of a Marx-type generator (operated at ~100 kV), a beam-forming diode utilizing a velvet cathode, a plasma chamber, and a short transport section employing solenoidal magnetic lenses to focus the electron beam from the diode to the plasma chamber. A single klystron-type cavity is placed downstream of the plasma chamber in some cases to measure beam coupling and energy extraction. In other cases, beam modulation is measured directly using a small Faraday cup collector that can be positioned at various axial positions, either inside or outside the plasma chamber.

The plasma is created by electrons emitted from a heated filament wound around the periphery of the 30-cm-diameter plasma chamber. Typically, argon gas is used as the neutral fill. Plasma density is measured with a Langmuir probe that

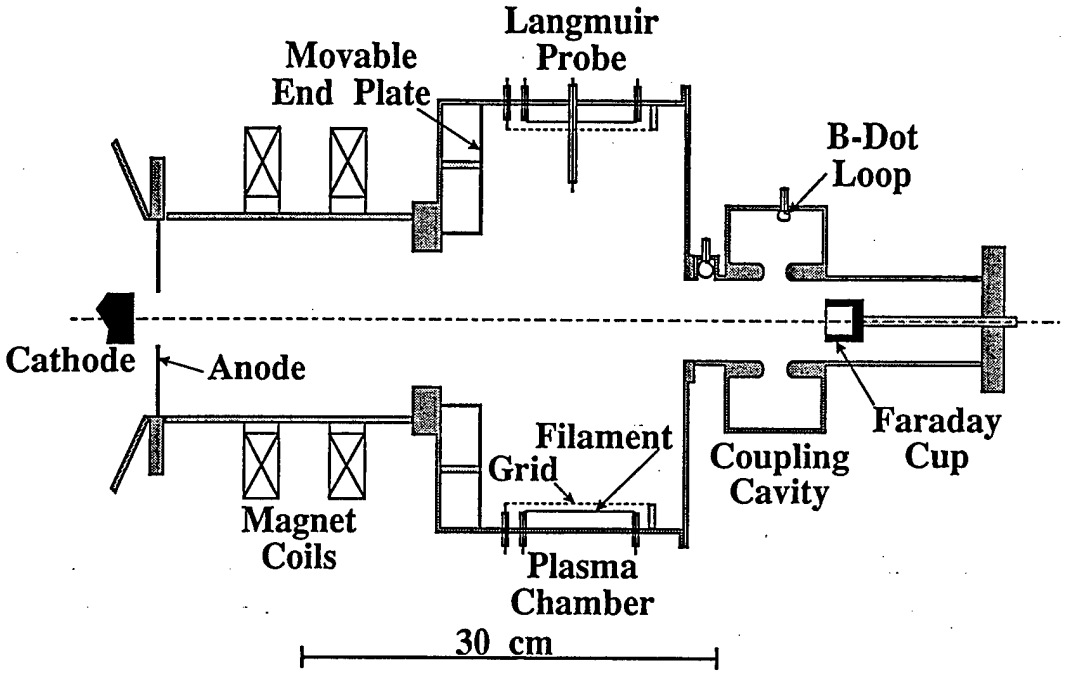

Figure 12. Experimental configuration.

can be moved radially or axially in the chamber. In normal operation, the Langmuir probe is positioned well off axis, and the density on axis is inferred from density scans obtained without the electron beam.

The measured density profile (without the electron beam) is shown in Fig. 13. In the upper graph, variation with radius is shown at the midplane of the cavity. The density is quite uniform out to a radius of about 8 cm. The axial variation, shown in the lower graph, is somewhat larger, at least on the tube axis where this scan was made. This is not surprising, because plasma is lost out the ends of the cavity. Although in principle some external plasma confinement scheme could be implemented to reduce this loss, it is important that radial electron motion not be impeded in the plasma chamber. Thus, magnetic mirror confinement is not feasible. Some thought was given to the use of electrostatic confinement, e.g., using a biased grid across the cavity openings; but because strong beam bunching was observed without any additional plasma confinement, no external confinement schemes were ever tested.

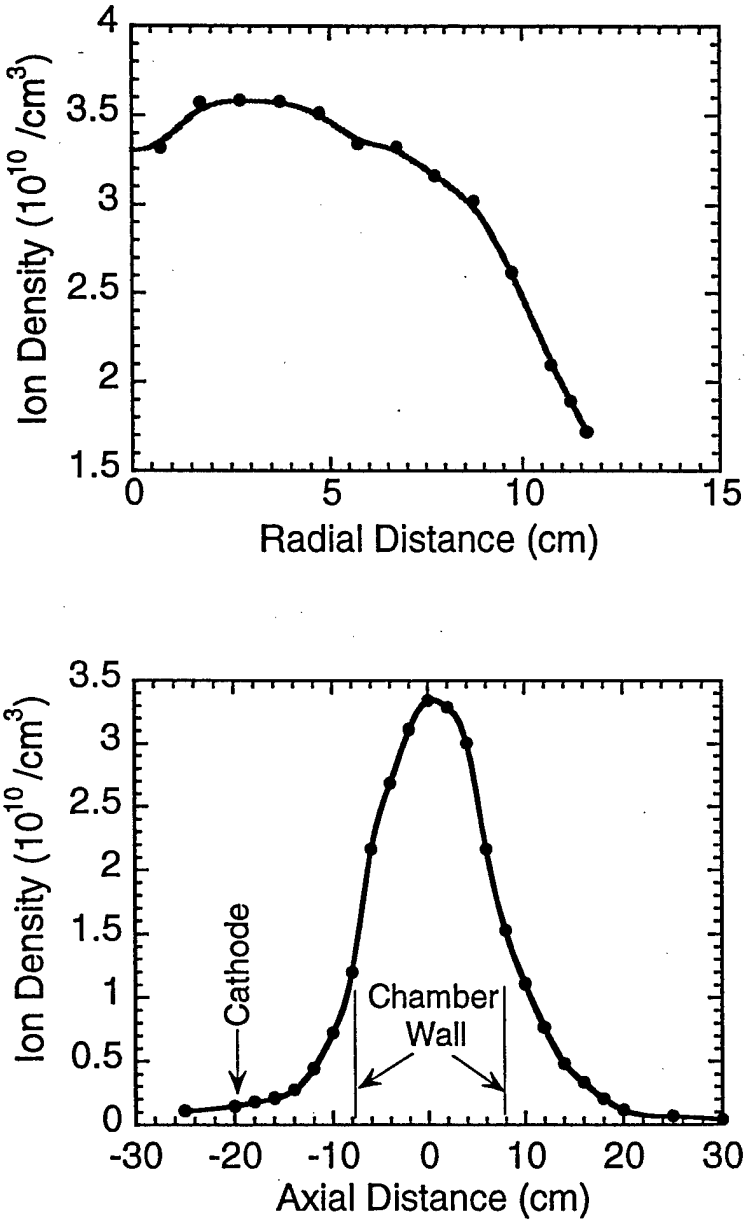

Figure 13. Measured plasma density profiles.

This POP device uses a pre-existing beam diode and plasma chamber, which physically could not be located any closer together than shown in the diagram. To transport the beam from the anode to the plasma chamber, we elected to use two opposing, flux-shielded solenoidal coils (B ~ 400 G) as opposed to an IFR plasma channel, which would have required a laser or a second, low-current electron gun to preionize the channel. The magnetic transport system was designed so that the beam was born in a field null and matched into the plasma chamber with minimal radial velocity. Thus, the beam could be extracted from the field and into the plasma without introducing a rotational velocity component (which would be

required to conserve canonical angular momentum if the cathode were located in the axial magnetic field). No focusing (other than that provided by the plasma itself) is provided downstream of the two solenoidal coils in the POP device, although if an extended extractor were to be used for maximum output power and/or bandwidth, auxiliary focusing would be required.

With this transport system, approximately 250 A of beam current was transported from the anode to the plasma chamber. This represents about half the total diode current. Although anode losses could account for some current loss, most of the current was lost radially within a few centimeters of the anode, and probably was due to electrons originating near the edge of the cathode with significant radial velocity. Because the 250 A was sufficient for our experiments, no attempt was made to replace the planar cathode with a Pierce-type concave cathode to obtain more efficient matching of the diode current into the magnetic transport region.

Figure 14 shows pertinent waveforms from the experiment, illustrating that the beam is strongly bunched in the plasma chamber. The diode voltage and current are shown along with the beam current at the downstream edge of the plasma chamber. The voltage and current waveforms consist of an initial plateau region of 100 to 150 nsec duration followed by a lower energy, lower current tail that persists for an additional 200 nsec. Normal and expanded views of the modulated current are shown. To determine the bunching frequency, the modulated current is measured on a fast analog scope (Tektronix 7904) on an expanded time scale (so that only a portion of the total waveform can be monitored on a given shot). This expanded waveform is then digitized using a Tektronix digitizing camera, and an FFT of the digitized trace is performed. These waveforms show that even though the injected beam varies in both energy and current, the beam is strongly bunched in the plasma chamber, with a high degree of coherence, and the modulation persists throughout the plateau portion of the voltage pulse.

The experimental results are summarized in Figs. 15 and 16. Fig. 15 shows the measured beam transport through the cavity and the oscillation frequency as a function of plasma density. Here, the plasma density as measured near the edge of the plasma chamber has been extrapolated to the center of the chamber using the Langmuir probe scans shown in Fig. 13. It is estimated that there is a $\pm 15\%$ uncertainty in this extrapolation, based on repeatability of measurements performed specifically to check the extrapolation. This uncertainty in plasma density is probably the largest contributor to scatter in the data and departure from the theoretical prediction. These measurements were made using Faraday cups

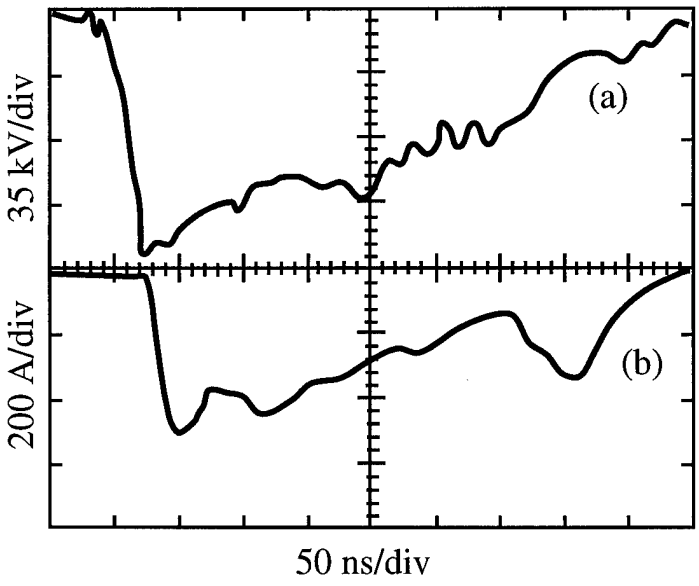

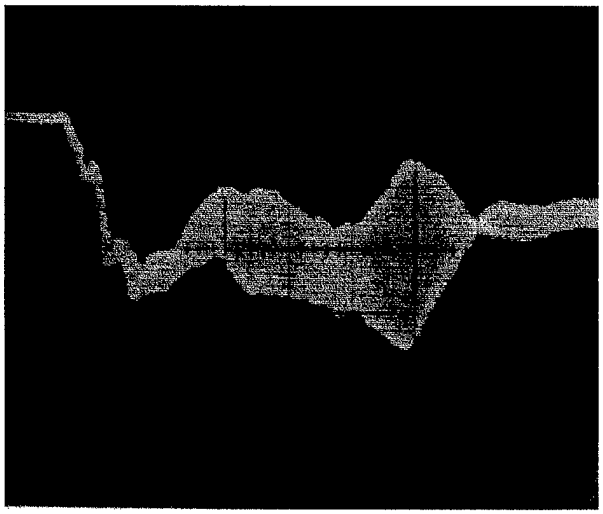

Figure 14. (a) Diode voltage. (b) Diode current. (c) Beam current at downstream end of plasma chamber.

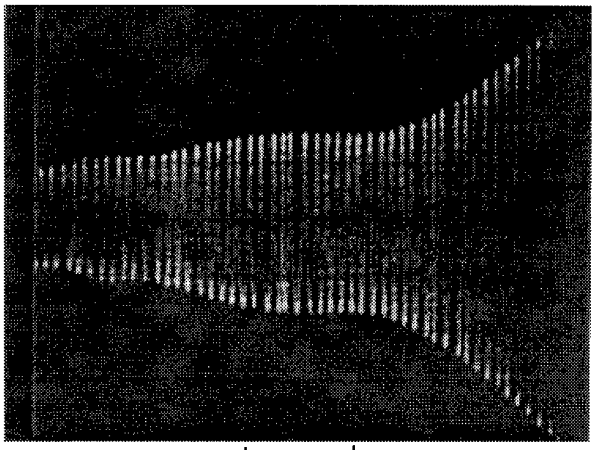

| 10 ns |

(d)

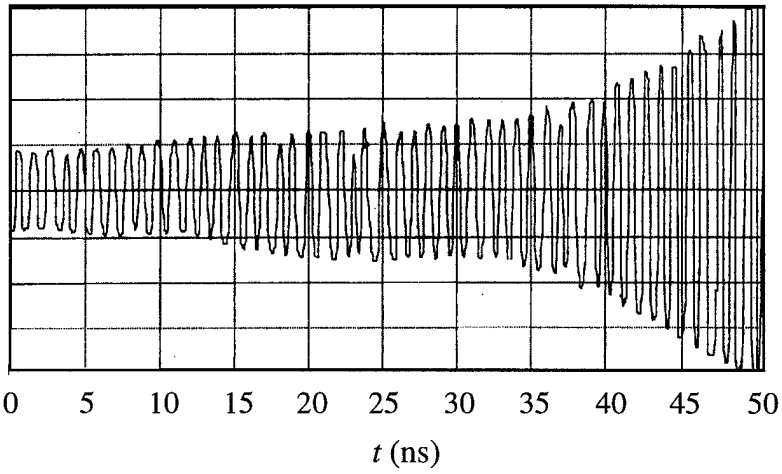

(e)

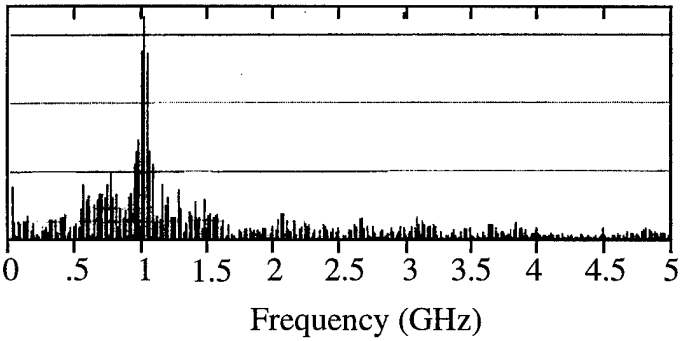

(f)

Figure 14. (d) Expanded view of modulated beam current. (e) Digitized version of waveform in (d). (f) FFT of waveform in (d).

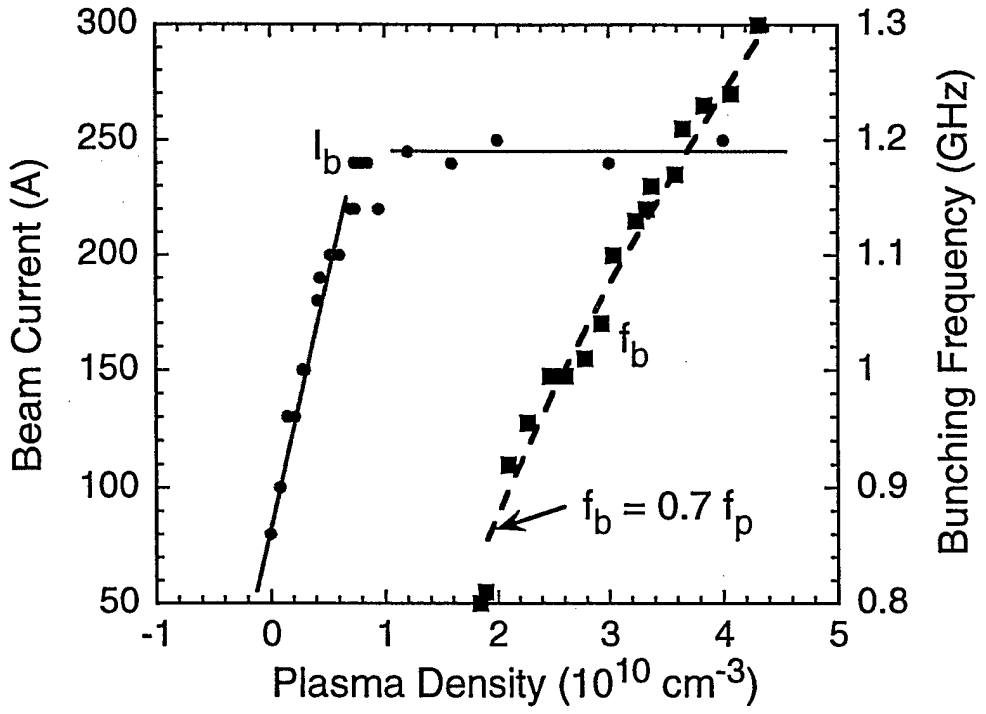

Figure 15. Beam transport through the plasma chamber and oscillation frequency vs. plasma density.

inserted axially into the system via semi-rigid coaxial cable inside a water-cooled sleeve. Total current was measured using a 7.6-cm-diameter collector. Essentially all the beam current was transported through the plasma chamber when the plasma density at the center of the chamber exceeded 7×10^9 cm^{-3}. At lower values of plasma density, the transported current decreased linearly to about 75 A with no plasma.

To obtain a better measure of the beam bunching, a small, low-inductance Faraday cup was used. This device, provided by Dr. Mark Litz of the Army Research Laboratory, was fabricated from an SMA connector, with a collector attached to the center pin and an aperture plate attached to the body of the connector. Aperture diameters of 1 to 3 mm were used. The frequency response of this collector was well in excess of the ~1-GHz bunching frequency observed in the experiment. The theoretical scaling of bunching frequency with plasma density is shown with the dashed line. The agreement is extremely good, with no free parameters used in the fit.

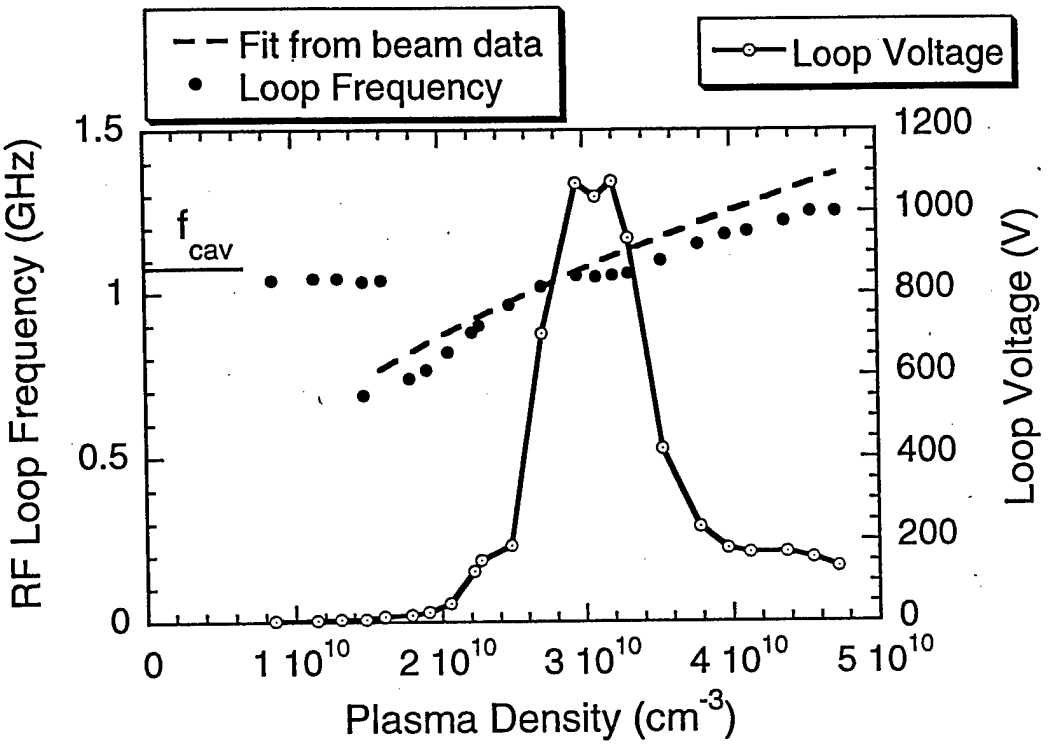

Figure 16. Cavity excitation frequency and amplitude vs. plasma density. A fit to the beam modulation frequency from Fig. 15 is superimposed.

Figure 16 is a combination plot showing the excitation of the downstream cavity together with the beam bunching frequency. Significant cavity excitation, as measured by a small probe inserted into the cavity, was observed only when the plasma density was adjusted to induce beam bunching at a frequency near the cavity resonance (measured at 1.08 GHz in cold tests). This is shown by the open circle data points, which peak at an ion density of about 3×10^{10} cm^{-3}. The solid circle data points represent the cavity oscillation frequency measured on the same shot as the loop voltage. The dashed line is a least squares fit to the beam bunching data measured at the output of the plasma chamber without the cavity, as shown in Fig. 15. With the exception of the very low level oscillations at the cavity resonance that were seen at the lowest values of plasma density, the RF loop response agreed very well with the previously measured beam bunching.

The width of the cavity excitation curve is somewhat broader than might be expected from the measured Q of the cavity. The FWHM of the excitation curve

corresponds to a variation of ~160 MHz in beam bunching frequency, whereas the cavity bandwidth (as measured in cold tests) is ~2 MHz (Q ~ 500). A careful examination of the data in Fig. 16 shows that the actual frequency measured from the loop in the cavity varies less than the beam bunching frequency in the region of strong excitation, but still much more than 2 MHz. Possible explanations for this behavior include a decrease in the cavity Q in the presence of the electron beam and possible feedback between the cavity and the plasma bunching chamber, thereby affecting the bunching frequency. Although the diameter of the drift region between the plasma chamber and the cavity is well below the value required to cut off all electromagnetic modes at the resonant frequency, the distance is only a fraction of a wavelength, so some evanescent feedback is possible.

The RF cavity was not optimized for extraction of energy from the beam. Nonetheless, a calibrated probe was used in conjunction with the widely-used RF cavity code, SUPERFISH, to determine the energy extraction. The field distribution as calculated by SUPERFISH is shown in Fig. 17. The RF magnetic field amplitude at the wall of the cavity was measured experimentally to be 250 G at saturation. With this field value as a normalization, SUPERFISH computes a stored energy of 0.2 J. This represents about 10% of the beam energy over the ~100-nsec growth time of the cavity field. This value is consistent with the MAGIC simulation results.

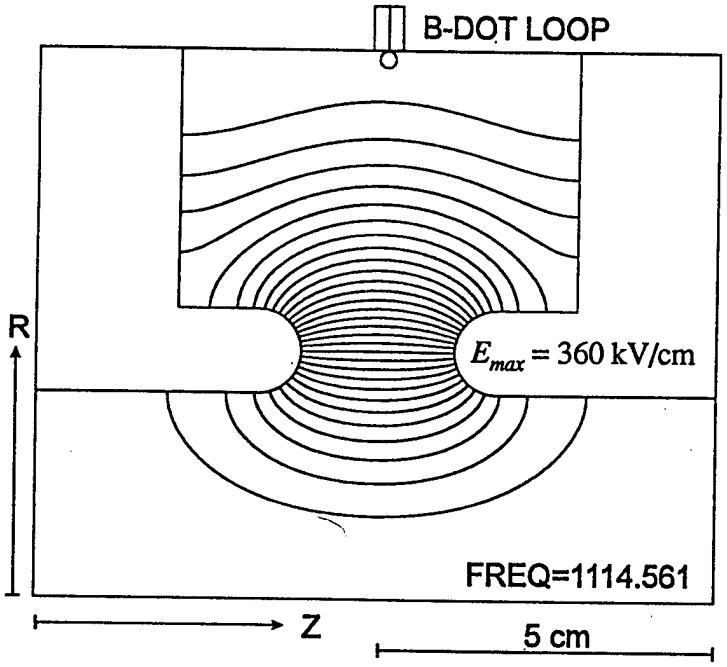

Figure 17. SUPERFISH analysis of RF extraction cavity.

5. DISCUSSION

The proof-of-principle experiment has demonstrated the plasma wakefield mechanism to be quite robust. Based on the experiments and simulations, the mechanism can produce intense modulation over a very wide range of beam parameters. The bunched beam that results from this axial modulation is well suited to RF energy production via interaction with standard microwave extraction structures. A single, non-optimized extraction cavity has converted about 10% of the beam energy to RF radiation. Based on simulations, a more complex, multiple-gap extraction structure should be capable of efficiencies on the order of 50%. Several important issues remain to be addressed in future work, however.

Clearly, to take advantage of the wide tunability of the device, a traveling wave structure or similar broad band circuit should be substituted for the simple klystron cavity used in the proof-of-principle experiment. Also, the stability of the device over long pulse durations, particularly at high power levels, remains an open question. Although, as shown in Fig. 14, we obtained data in which the beam modulation was stable for essentially the full duration of the main voltage plateau, there were some cases in which the modulation terminated suddenly and prior to the end of the voltage plateau. Examples are shown in the Appendix. On most of these short-pulse shots, but not all, some anomalous behavior was evident in the diode voltage or current waveforms, such as a dip in voltage or injected current that could be caused by a gun arc. A more stable pulse generator having a flatter output pulse is required to address this issue adequately.

APPENDIX

In this appendix, we present some additional examples and details of the experimental effort. The results in the body of the report were typical, and the summary plots presented the results of a large number of shots. However, a number of anomalous effects were observed that we currently cannot explain. It is likely that the relatively poor quality (flatness) of the diode voltage and current contribute to these effects, but there could also be problems associated with plasma formation (e.g., uniformity or timing) on some of the shots. In any case, for completeness we will include examples of some of this anomalous behavior.

In most cases, the FFT of the bunching or cavity excitation waveforms was quite clean, with little harmonic content. In about 10% of the shots, however, there was a different type of bunching, with significant first harmonic content. We could not determine any particular reason for this different behavior. An example of the Faraday cup current waveform and its FFT for a shot of this type are shown below.

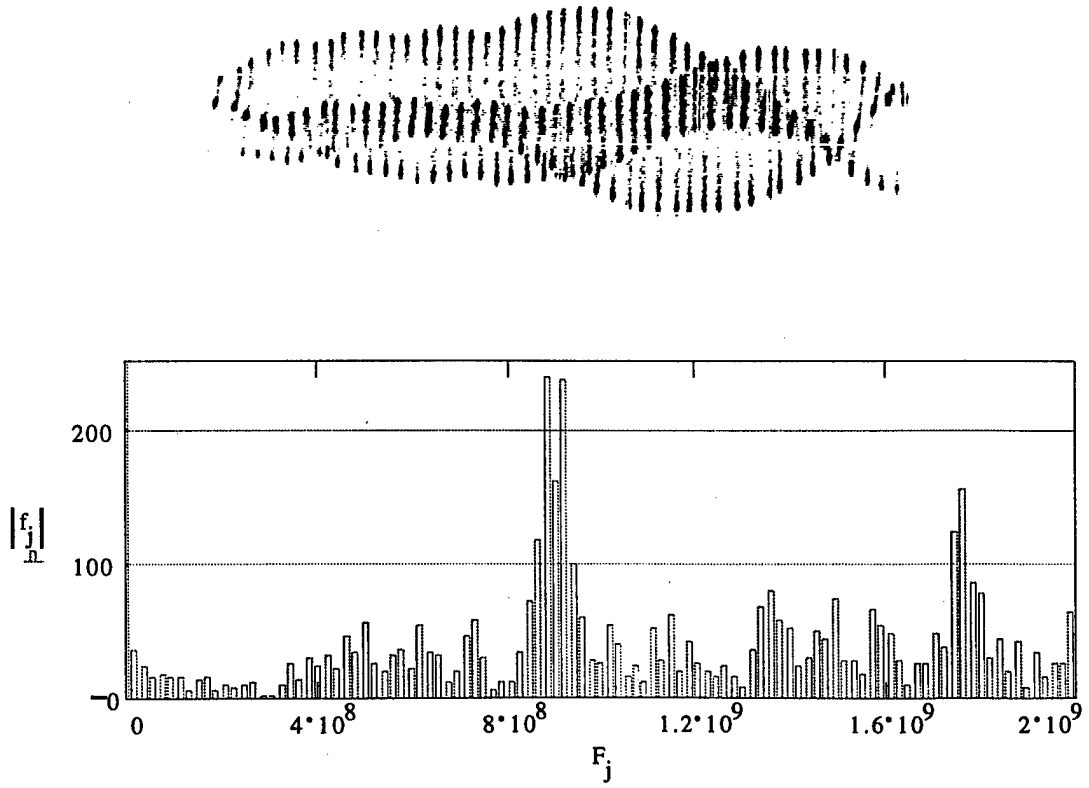

Figure A1. Current waveform and FFT illustrating output at first harmonic.

On a few shots with the extraction cavity, the output spectrum consisted of two well-defined frequencies, with the higher frequency about 1.5 times the lower one. The higher frequency was at the cavity resonance, and the lower one was about the value expected from the plasma frequency. The signal levels here were about 40 dB below the peak values measured when the plasma frequency coincided with the cavity resonance, so the effect is interesting but not very important. An example of this behavior is shown in Fig. A2.

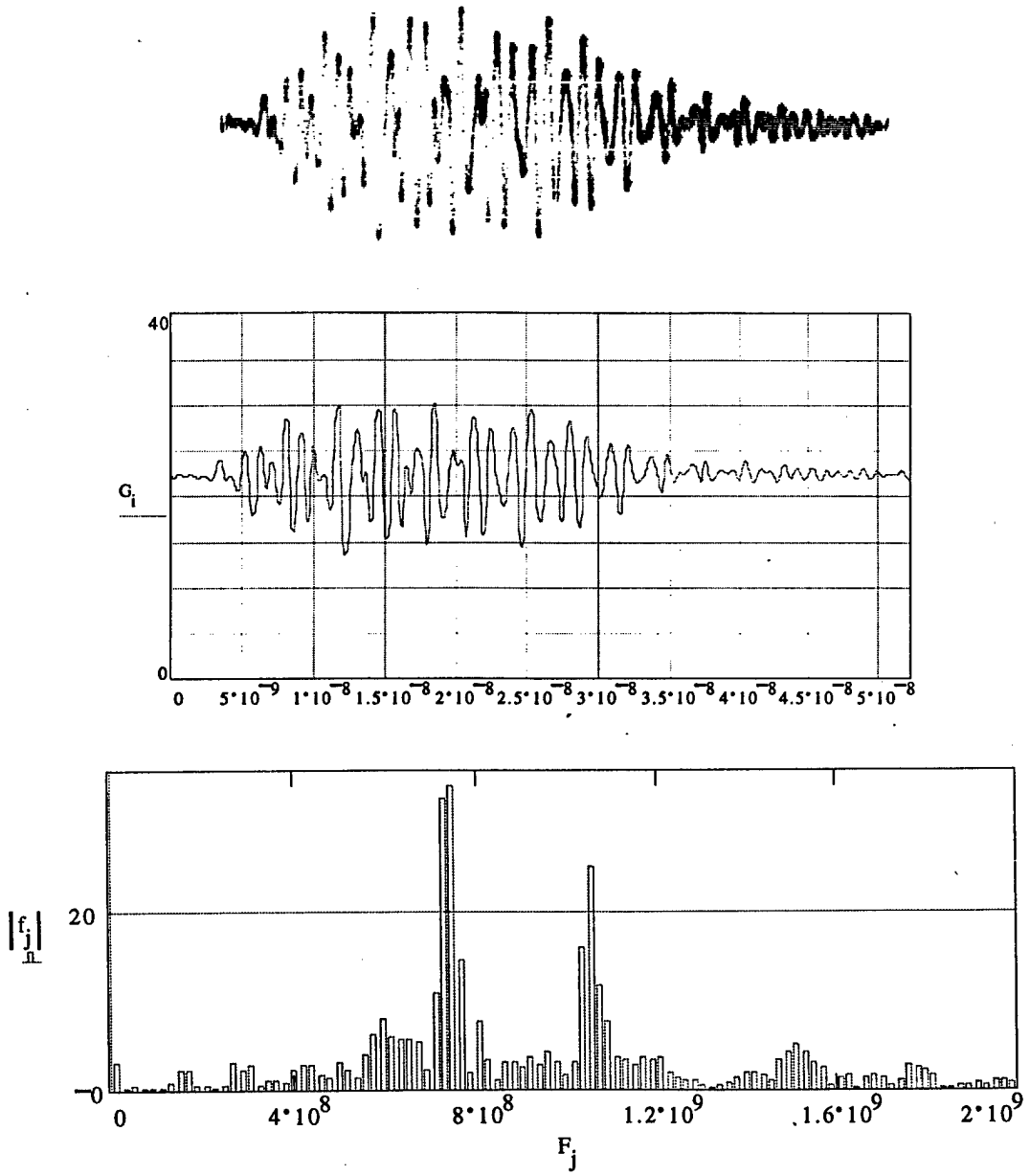

Figure A2. Cavity excitation with the plasma frequency well below resonance. Top: Raw waveform. Middle: Digitized waveform. Bottom: FFT.

At the highest RF power levels in the cavity, the output waveforms indicated that breakdown might be occurring. Looked at on a long time scale, the output grew rapidly, then suddenly dropped. Sometimes, but rarely, the drop was followed by another increase to a level approaching the first peak. Several examples are shown in Fig. A3, all at 50 nsec/div.

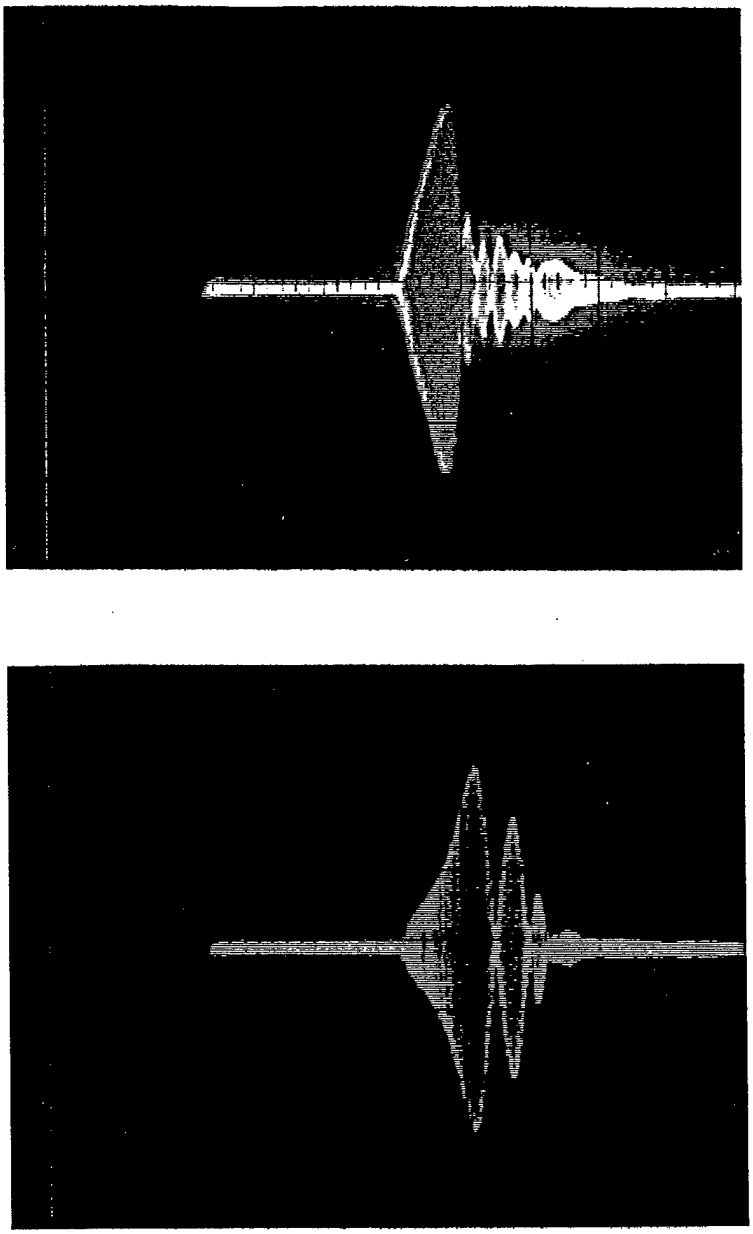

Figure A3. Examples of cavity waveforms where breakdown might be occurring. Horizontal scale: 50 nsec/div.

Large variations in beam bunching amplitude inside the plasma chamber were sometimes observed during a pulse. Occasionally, the bunching would begin early in the pulse and then die out, with little bunching for the remainder of the pulse. There seemed to be a stronger likelihood of this behavior at higher plasma frequencies. Examples of this behavior are shown in Fig. A4.

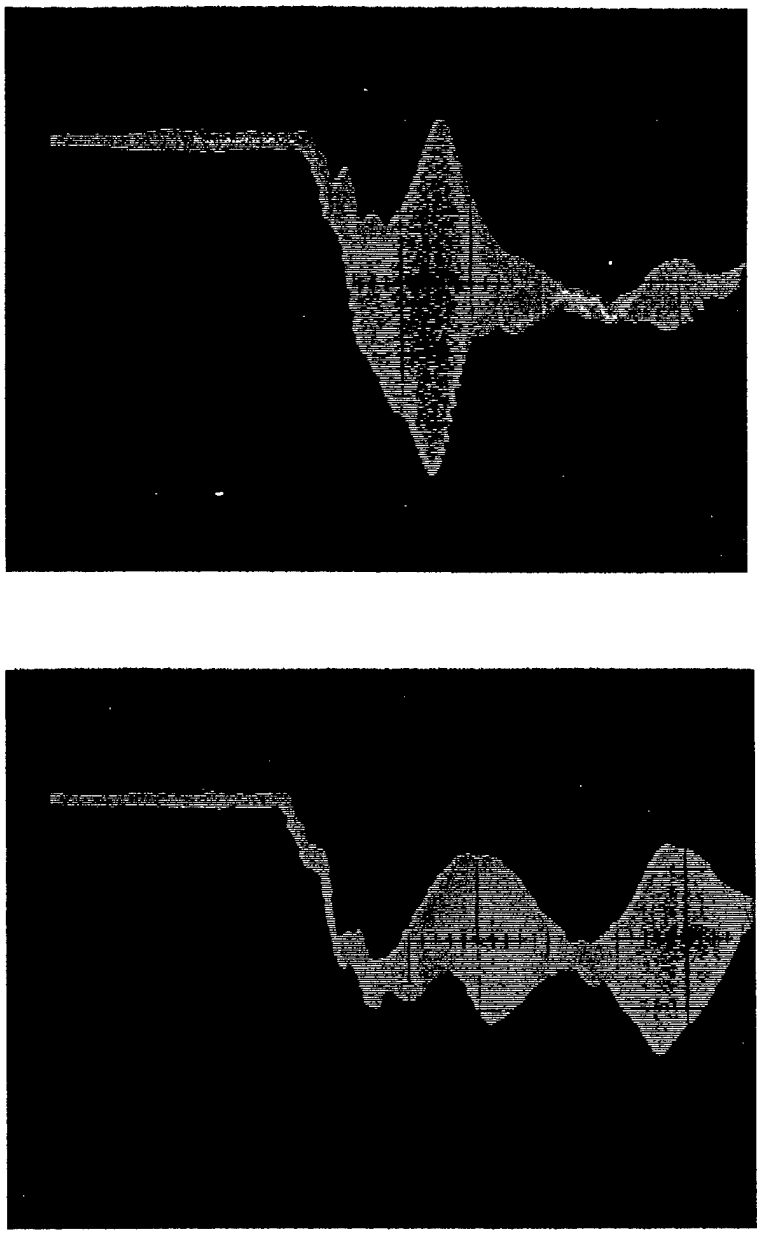

Figure A4. Examples of Faraday cup waveforms where bunching terminates prematurely. Horizontal scale: 20 nsec/div.

Finally, the experimental hardware was fabricated primarily from existing components that were not optimal for the PWK. The plasma chamber was located inside a much larger vacuum chamber. A scale drawing of the overall experimental hardware is shown in Fig. A5. Not shown here are the various ports used to insert probes and the Faraday cups. Ports were located in the outer wall as well as in the downstream end plate.

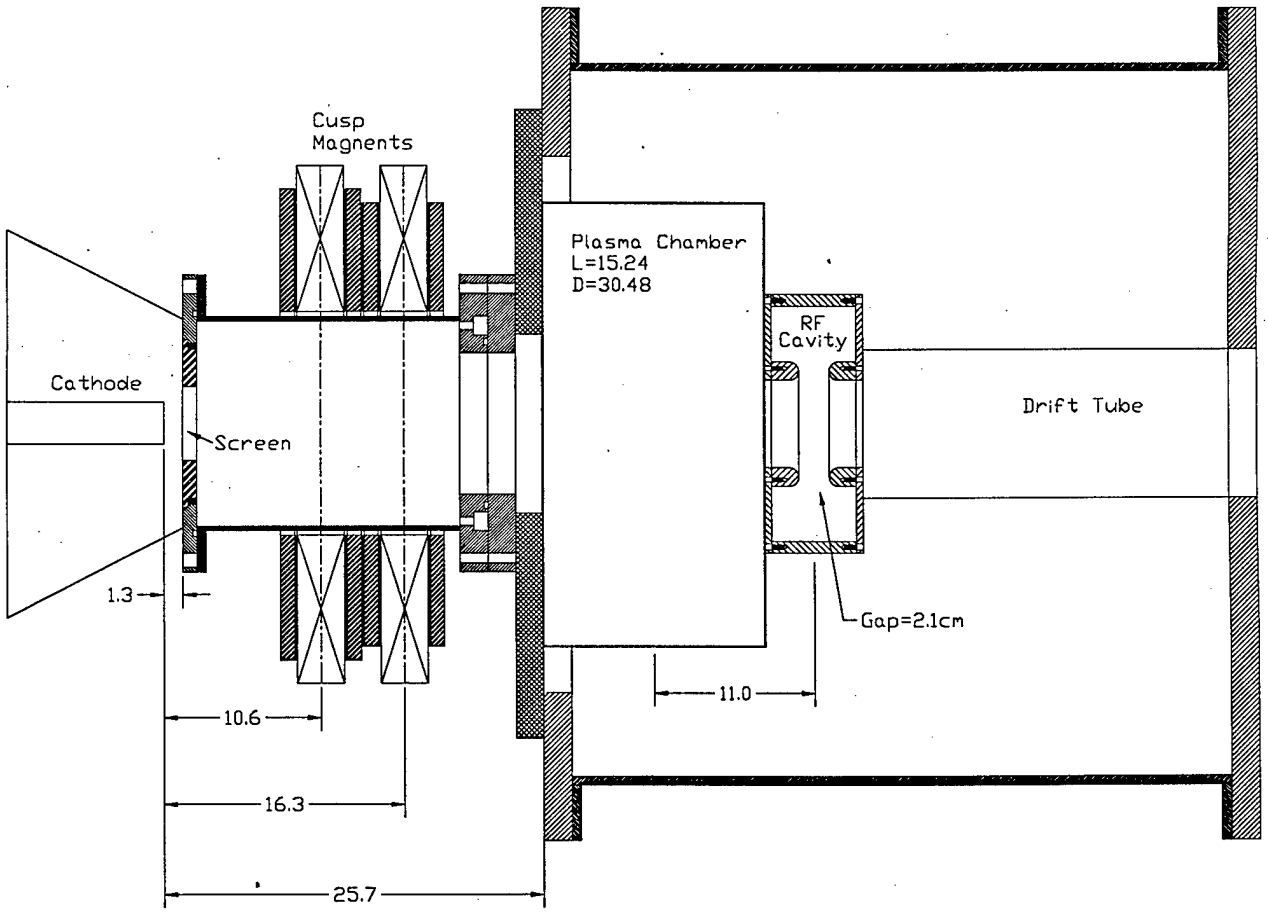

Figure A5. Overall scale drawing of the experimental apparatus. Dimensions are in cm.

[1] J.D. Miller, R.F. Schneider, D.J. Weidman, H.S. Uhm, and K.T. Nguyen, "Plasma Wakefield Effects on High Current REB Transport in the Ion-Focused Regime," Phys. Fluids B **4**, 4121 (1992).

[2] G. Caporaso, F. Rainer, W. Martin, D. Prono, and A. Cole, "Laser Guiding of Electron Beams in the Advanced Test Accelerator," Physical Review Letters, **57**, 1591, September 1986.

[3] S.L. Shope, C.A. Frost, G.Leifeste, and J.W. Poukey, Phys. Rev. Lett. **58**, 551 (1987).

[4] J.D. Miller, R.F.Schneider, D. Weidman, H. Uhm, and K.T. Nguyen, Phys. Rev. Lett. **67**, 1747 (1991).

[5] T.C. Katsouleas, C. Clayton, L. Serafini, C. Pellegrini, C. Joshi, J. Dawson, and P. Castellano, IEEE Trans. Plasma Sci. **24**, 443 (1996).

[6] B. Goplen, L. Ludeking, D. Smithe, and G. Warren, "User-Configurable MAGIC for Electromagnetic PIC Calculations," Comp. Phys. Comm. **87,** 54 (1995).

[7] Nicholas A. Krall and Alvin W. Trivelpiece, Principles of Plasma Physics, San Francisco press, 1986, Chapter 4.

[8] G.M. Branch and T.G. Miran, "Plasma Frequency Reduction Factors in Electron Beams," IRE Transactions-Electron Devices, 1955, pg. 3.

[9] M. Friedman, J. Krall, Y.Y. Lau, and V. Serlin, "Externally Modulated Intense Relativistic Electron Beams," Journal of Applied Physics **64**, 3353 (1988).